# An experimental study of the influence of particle size heterogeneity on seismic wave velocities

Jules Marti, Santiago Quinteros, T. Dylan Mikesell, Ludovic Margerin, Pierre Delage, Naomi Murdoch

# An experimental study of the influence of particle size heterogeneity on seismic wave velocities

Jules Marti[1], Santiago Quinteros[2],
T. Dylan Mikesell[3], Ludovic Margerin[4], Pierre Delage[5], and Naomi Murdoch[6]

[1]Institut Supérieur
de l'Aéronautique et de l'Espace (ISAE-SUPAERO), Université de Toulouse, Toulouse, France & Institut de recherche
en Astrophysique et Planétologie, Université de Toulouse, CNRS, Toulouse, France; email : jules.marti@irap.omp.eu

[2]Norwegian Geotechnical Institute, NGI, Oslo, Norway; email : Santiago.Quinteros@ngi.no

[3]Norwegian Geotechnical Institute, NGI, Oslo, Norway; email : dylan.mikesell@ngi.no

[4]Institut de recherche
en Astrophysique et Planétologie, Université de Toulouse, CNRS, Toulouse, France; email : Ludovic.Margerin@irap.omp.eu

[5]Ecole des Ponts ParisTech, Laboratoire Navier/CERMES, CNRS, Marne la Vallée, France; email : pierre.delage@enpc.fr

[6]Institut Supérieur de l'Aéronautique
et de l'Espace (ISAE-SUPAERO), Université de Toulouse, Toulouse, France; email : Naomi.MURDOCH@isae-supaero.fr

## Abstract

Seismometers on board the Apollo and InSight missions measured seismic wave velocities in lunar and Martian surface material (i.e., regolith). As on Earth, these regoliths have different grain size distributions. To better interpret these in-situ seismic observations we conducted laboratory experiments to investigate the role of grain size heterogeneity on seismic wave velocity. Our experiments use piezoelectric bender elements to excite and measure seismic wave propagation through samples comprised of binary mixes of glass beads. We propose a physical explanation of the experimental observations, which cannot be attributed to bulk density variations alone. To isolate the effect of grain size distribution, 14 binary mixes were intentionally designed with different grain size distributions, and our results indicate that two mechanisms influence the sample microstructure depending on grain size distribution: hole filling and contact rupture. While the former leads to increases in seismic velocity, the latter does the opposite. Consequently, particle size heterogeneity should be considered when investigating seismic wave velocities in planetary surfaces.

## 1 Introduction

Measuring seismic wave velocities is a widely-used non-destructive technique to investigate the elastic properties of different materials (e.g., Bay et al. 1992). By examining the seismic velocity we gain important insights into properties like density, in addition to the bulk elastic properties (e.g., Young's modulus, shear modulus; Robertson et al. 1986; Mayne 2014). This investigative method is employed in both laboratory and field settings, making it a versatile tool for geophysical and geotechnical analyses alike (Viggiani et al. 1995; Christensen et al. 1995; Holbrook et al. 1992; Mayne 2014).

The use of seismometers on Earth's surface has enabled the investigation of the Earth's structure, from the crust to the core in an objective manner (e.g., Brune et al. 1963). Seismometers have also been utilized in extraterrestrial missions, including the Moon and Mars. For example, the geophones that were carried onboard the Apollo missions (Nakamura et al. 1982) gathered continuous seismic data for a duration of 8 years, while the SEIS instrument (Lognonné et al. 2019) was deployed on Mars at Elysium Planitia by

the InSight mission (Banerdt et al. 2020; Giardini et al. 2020) and collected seismic data for two Martian years, which is equivalent to almost four Earth years.

Both, the Apollo and InSight instruments were positioned on the surfaces of the Moon and Mars, respectively, on top of the planetary regolith. Regolith refers to the unconsolidated material that covers competent bedrock, and is created by impact gardening, weathering, erosion, transport, deposition, or cratering of older material (Eggleton 2001). Since this layer is in direct contact with seismometers, any seismic wave that has been recorded by the seismometers must travel through the regolith layer (Fayon et al. 2018). Local wave velocities have been measured by Brinkman et al. (2022) at the InSight landing site, and are in reasonable agreement with laboratory measurement on loose regolith simulants (Delage et al. 2017). It is, therefore, of significant interest to have a clear understanding of the propagation of seismic waves in these materials.

Meteorite impacts on the Moon generate an angular regolith with a large variety of grain sizes (McGlynn et al. 2011). Hence, 90% of the regolith mass comprises grains between $10^{-5}$ to $10^{-3}$ m in size (Carrier 2003). Unlike the Lunar regolith grain size distributions analysed from returned samples, Martian regolith grain size distribution estimates are limited by instrument resolution. Data from various missions indicate that the bulk of the material on Mars consists of less angular wind-rounded particles ranging in size from $10^{-5}$ to $10^{-4}$ m, with a resolution of $10^{-7}$ m (Golombek et al. 2020; Herkenhoff et al. 2008). This provides only an estimate of the average particle size distribution on Mars. However, McGlynn et al. (2011) demonstrates that the local distribution of particle size is highly diverse and dependent on aeolian processes. Additionally, a diversity of grain size distributions exists on Earth (e.g., Cho et al. 2006) or on asteroids (e.g., Murdoch et al. 2015), as a result of various processes including saltation, erosion, weathering, gravity sorting, aeolian processes, and meteoroid impacts. Therefore, grain size distribution analysis should be considered as it provides a basic understanding of particles formation processes and insights into the studied celestial bodies (Verdier et al. 2023; McGlynn et al. 2011; Goetz et al. 2010).

Investigating the impact of grain size distribution on the velocity of seismic waves is a topic of significance for both current and upcoming missions. Examples include the Farside Seismic Suite, which intends to position a seismometer on the farside surface of the Moon, as well as the seismic instrumentation intended to function on the surfaces of asteroids (Murdoch et al. 2017; Murdoch et al. 2023; Bernauer et al. 2020). The novelty of the work presented herein lies in the systematic investigation of the effects of grain size distribution on the velocity of seismic waves. For this purpose, we have carried out laboratory experiments varying the grain size ratio of smaller and larger particles and the mass fraction of small particles.To the best of our knowledge, the grain size distributions investigated in this research have not been studied in previous work. These experiments, therefore, provide seismic velocity data in an extended measurement range allowing us to observe velocity variations with grain size distribution, and to suggest some new microstructural interpretations to explain the observations. Although relevant, angularity and gravity effect are not studied in this framework. In Section 2 we introduce the experimental design, and in Section 3 we present the experimentally observed velocity variations, which depend on the grain size distribution. In Section 4 we present our interpretations and consider the physics at the grain scale. In Section 5 we discuss the protocol and implications of our work.

# 2 Experimental design

## 2.1 Samples

The granular material tested is a binary mixture of silica glass beads. Beads have been chosen to facilitate future numerical discrete element model simulations (Sunday et al. 2020). While bead material does have

an effect on absolute seismic velocities (Zimmer 2004), because we use the same type of glass beads with different diameters, we are able to isolate the effect of grain size distribution on seismic velocity. Importantly, the sizes of the beads were sufficiently characterized by the manufacturer so that we did not need to measure the grain size distributions by ourselves.

We use two parameters to characterise the studied mixtures. The first, called Grain Size Ratio (GSR), is defined as $GSR = d_S/d_L$, where $d_S$ and $d_L$ are the diameters of the small and large beads, respectively. The second parameter is the Mass Fraction of the smaller beads (MF), which is defined as $MF = \frac{m_S}{m_S+m_L}$, where $m_S$ and $m_L$ are the masses of the small and large beads, respectively. Four different bead diameter ranges were used: 300-355 $\mu$m, 600-710 $\mu$m, 800-850 $\mu$m, and 2500-2800 $\mu$m. The largest beads were selected to ensure that there were at least 10 particle diameters across the full sample diameter. The smaller bead sizes were then selected to provide the desired GSR with respect to the larger beads. As long as there is a large enough number of particles in the experiment to avoid boundary effects, the specific particle size should not influence the seismic velocity (Yang et al. 2012; Dutta et al. 2019), and we expect that results obtained in this study are applicable to soils with the same GSR but different diameters of small and large beads. The values of GRS and MFs investigated in this study are listed in Table 1.

| GSR | $d_S$ ($\mu$m) | $d_L$ ($\mu$m) | MF | | | | | |
|---|---|---|---|---|---|---|---|---|
| | | | 0.05 | 0.1 | 0.2 | 0.4 | 0.6 | 0.8 |
| 0.3 | 800-850 | 2500-2800 | X | X | X | X | | |
| 0.4 | 300-355 | 800-850 | | X | X | X | X | |
| 0.5 | 300-355 | 600-710 | | X | X | X | X | X |

Table 1: Grain Size Ratio (GSR) and Mass Fraction (MF) tested using small diameter ($d_S$) and large diameter ($d_L$) glass beads.

## 2.2 Experimental hardware

To measure seismic wave velocity, we use a bender element system. Bender elements consist of two polarised plates of piezoelectric material bonded together, which bend when a voltage is applied to them (Dyvik et al. 1985). If the wiring is switched from parallel to series and the polarisation is reversed, they can also produce an electrical signal when deformed (Lings et al. 2001). The bender elements used in this work are designed to produce shear (S) waves, but small-amplitude compression (P) waves are also generated. Care is taken in the analyses to focus on the S-waves (Camacho-Tauta et al. 2012).

To measure seismic waves propagating through the sample, emitting and receiving bender elements are positioned at each end of the cylindrical sample (Fig. 1). A sinusoidal pulse with a selected input frequency is sent to the emitting bender element and the seismic wave (in our case, the S-wave) propagates through the sample and is recorded by the receiving bender element. By analysing the waveform at the receiving bender, it is possible to calculate the time taken for the seismic wave to travel the known distance between the tips of the two bender elements.

The glass bead mixes are contained in a cylindrical latex membrane with a diameter of 5 cm and a height of 10 cm (ratio H/D = 2). The sample is mounted on top of a bottom pedestal containing the receiver bender element. The top of the pedestal is constructed from porous material, which enables the user to change the pressure inside the sample by applying a given level of vacuum, resulting in a pressure difference between the exterior (atmospheric pressure) and interior of the membrane. The confining pressure is quantified using a barometer located within the membrane. Two pressures were tested (25 kPa and 50 kPa). Fig. 1 shows the experimental set-up.

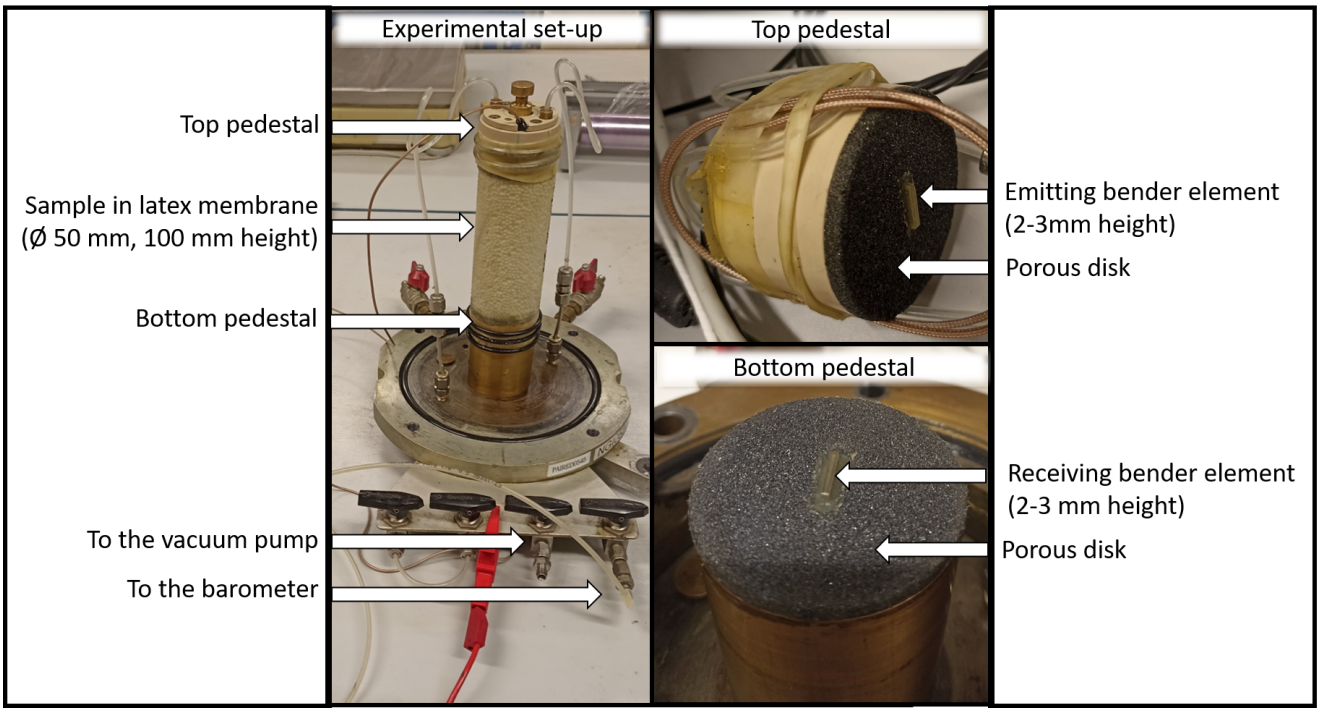


Figure 1: Experimental hardware.

## 2.3 Experimental Protocol

To prepare the specimens, we use an air-pluviation technique with a constant drop height. Specifically, we use a funnel filled with the bead mixture and raise the funnel by hand to maintain a constant drop height of two centimeters above the sample surface. When the sample container was half full, light tapping is applied for compaction purposes. This procedure enhances the contact between the bottom bender element and the beads. The same step is then repeated when the sample membrane is full. The air-pluviation method (Yamashita et al. 2009) is widely used in soil sciences, but it does have some limitations that are discussed in Section 5. To ensure the regular cylindrical specimen shape during filling, a splitting mold is placed around the membrane. A vacuum is applied between the membrane and the mold to bond the membrane to the mold. Once the sample has been filled, a partial vacuum of 20 kPa is applied inside the sample and the mould is subsequently split and carefully removed. The pressure level is then adjusted to 25 kPa or 50 kPa.

Prior to mounting, the specimen mass is measured with a digital scale, the specimen height is measured with a caliper, and the circumference of the sample is measured with a tape measure at three different heights along the cylinder. The total volume ($V_T$) is computed as $V_T = \frac{h}{3}\pi\sum(\frac{C_i}{2\pi} - e_i)^2$, where h is the specimen height, $C_i$ is the circumference at height i, and $e_i$ is the thickness of the membrane at corresponding locations measured prior to sample mounting. Bulk density is then estimated using the specimen mass and volume. Measurements errors on h, $C_i$ and $e_i$ are all included in the density error estimate, and we note that density is estimated at both confining pressures (25 kPa or 50 kPa).

A sinusoidal pulse is selected as the input signal for our experiments due to its widespread usage (Yamashita et al. 2009) and narrow frequency spectrum, which results in less distortion of the output signal compared to a square pulse (Blewett et al. 2000). The frequency range was chosen considering the dominant wavelength in the specimen, which should not exceed half of the sample height, following the guidelines proposed by Camacho-Tauta et al. (2012). Thus, the input frequency needs to be higher than 2V/h, where V is the shear wave velocity and h is the specimen height. As velocity is unknown in advance, this condition is investigated at a later stage. Tests are conducted with input frequencies from 2 to 20 kHz. However, for input frequencies greater than 10 kHz, the results are noisy and difficult to interpret. Before

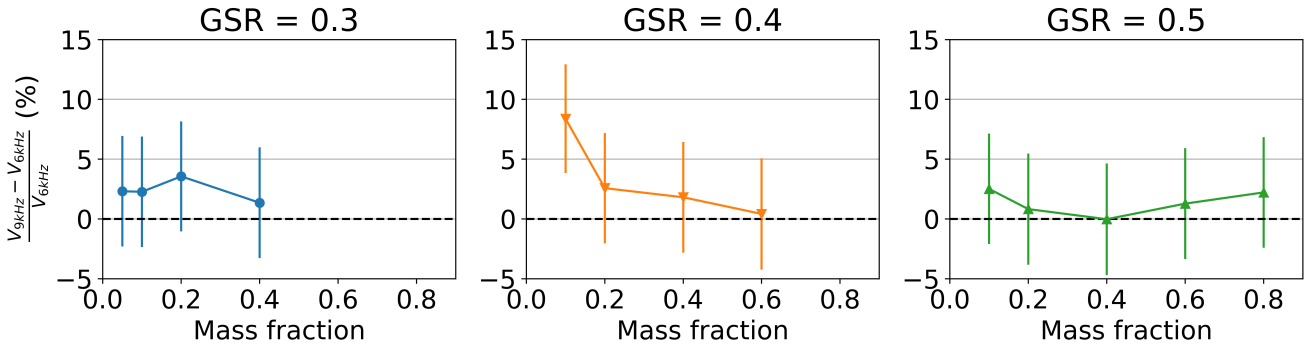


Figure 2: Evolution of the normalized velocity difference with GSR and MF at 50 kPa, where $V_{6kHz}$ and $V_{9kHz}$ are velocities obtained at 6 and 9 kHz, respectively. The error bars in velocity are estimated following Table 1 in Carotenuto et al. (2020).

mounting the sample, a reference measurement is taken with the two bender elements placed in contact to determine the system response time delay. This delay is then subtracted from the estimated arrival time during testing.

Velocity is measured using the peak-to-peak method (Yamashita et al. 2009). Following recommendations in Carotenuto et al. (2020), we search for the frequency providing the largest signal-to-noise ratio (SNR). In our case we find this to be 6 kHz. However, the impact of input frequency on the measured velocity is assessed in the next section. In addition, a 6 kHz input frequency guarantees that the sample length is greater than two wavelengths (Camacho-Tauta et al. 2012), and unless otherwise specified, all subsequent results are for an input frequency of 6 kHz. We note that using the optimal input frequency is critical to minimize uncertainty in the arrival time picking and corresponding velocity estimation. Carotenuto et al. (2020) determine that if the frequency used is within a reasonable range around the optimal frequency, then the maximum uncertainty in V due to frequency is less than 2%. Here we neglect this uncertainty, as well as the uncertainty due to measurement of the propagation distance (i.e., cylinder height, which is $<$0.01 mm). Instead, we consider the largest uncertainty, which is due to specimen preparation. We did not have time nor resources to replicate the experiments in our study. Thus, as a conservative uncertainty estimate, we follow the literature. Carotenuto et al. (2020) made multiple measurements on replicated samples using the exact same instrumentation and protocols as in this study. At 50 kPa Carotenuto et al. (2020) estimate the velocity uncertainty due to sample preparation is $\pm$3.3% (i.e., Table 1 in Carotenuto et al. 2020), and at 21 kPa Carotenuto et al. (2020) estimate the velocity uncertainty is 11.2%. We use these two values to compute the errors in our experiments at 50 and 25 kPa, respectively.

# 3 Results

First, as check on our assumptions about optimal frequency, we investigate the frequency dependence of the results. Fig. 2 presents the normalized differences in estimated velocities using 6 kHz and 9 kHz input frequencies. The small discrepancies ($<$5%) between the two datasets indicate that frequency does play a role in uncertainty, but along the lines of a few percent as shown in Carotenuto et al. (2020), even when we are well outside the optimal frequency range at 9 kHz. The only outlier is the high velocity value at GSR=0.4 and MF=0.1. For an input frequency of 9 kHz it appears that the velocity is higher, but given the measurement uncertainty it is not clear if this is significant.

Fig. 3 presents the S-wave velocity observations at 6 kHz as a function of GSR at different MFs for confining pressures of 25 kPa and 50 kPa. Several observations can be made: (i) at constant GSR and MF the velocity increases with pressure, as expected (Eberhart-Phillips et al. 1989), (ii) at GSR=0.3 the velocity increases with MF until MF=0.2 and then decreases at both pressure levels, (iii) at GSR=0.4 the velocity slightly increases with MF at both pressure levels, (iv) at GSR=0.5 the velocity decreases with

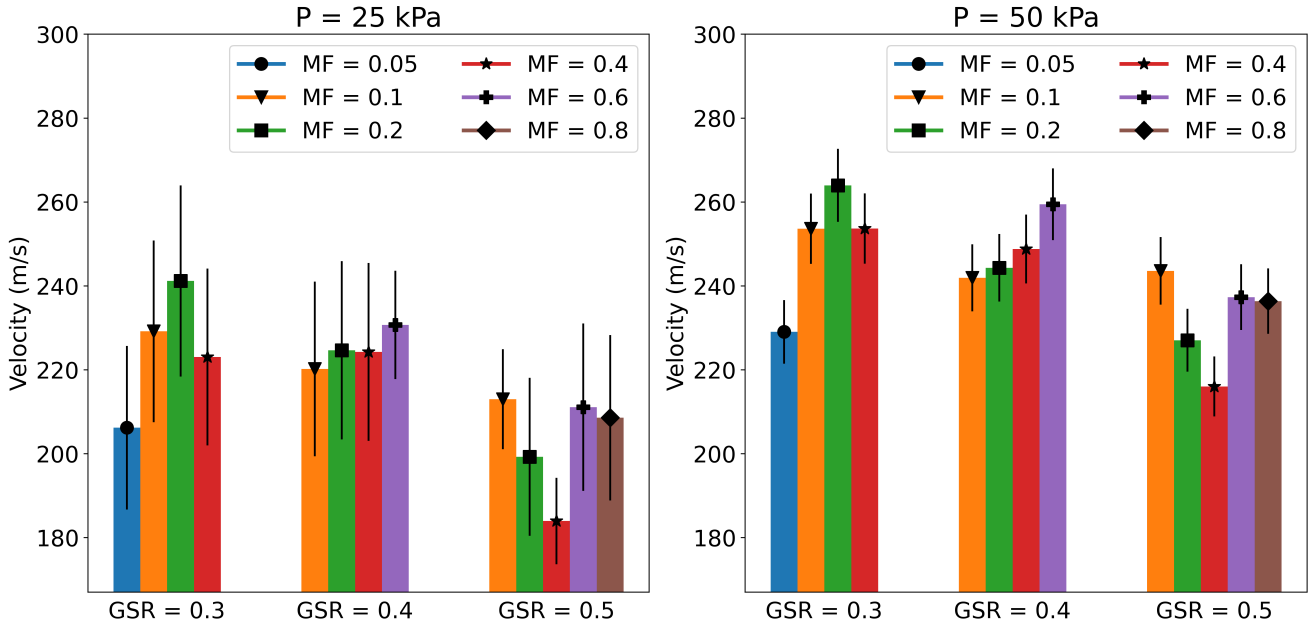


Figure 3: Evolution of S-wave velocity with GSR and MF at an input frequency of 6 kHz. The error bars in velocity are estimated following Table 1 in Carotenuto et al. (2020).

increasing MF until MF=0.4 and then velocity increases at both pressure levels, (v) at constant MF the velocity decreases with GSR at both pressure levels. These observations all hold within the estimated errors.

In elasticity theory the shear wave velocity (V) depends on the rigidity or shear modulus of the medium G and the density $\rho$ as $V^2 = G/\rho$ (Graff 1975). To identify if the observed velocity variations in our granular samples are density related or macroscopic ridigity related we assess the data as a function of density (Fig. 4). The left plot shows the measured densities for the different samples at 50 kPa confining pressure. The density increases steeply with MF at GSR=0.3 and GSR=0.4 up to MF$\leq$0.2. A slight increase in density with MF is observed at GSR=0.5 for MF$\leq$0.4, followed by a slight decrease for MF>0.4. Density remains almost constant otherwise. Results for at 25 kPa confining pressure are not shown, but they are similar to those at 50 kPa.

To investigate whether the observed velocities are impacted solely by density, Fig. 4 also illustrates the evolution of both velocity and density. Consider first the cases of GSR=0.3 and GSR=0.4. Both density and velocity increase with MF, except for the highest MF value tested in GSR=0.3. However, in the case of GSR=0.5, there is a negative correlation between the velocity and the density as MF increases. Therefore, we speculate that density alone cannot explain all the observed velocity variations.

# 4 Proposed interpretations

## 4.1 Microstructural considerations

Here we propose possible physical mechanisms that may be responsible for the observed variations of seismic velocity with mass fraction (MF) and grain size ratio (GSR). At low MF (i.e. small quantities of smaller beads), the skeleton of the medium is mainly composed of large beads for all grain size ratios. Consequently, the small beads have a negligible influence on the seismic wave propagation (Fig. 5a,e). At high MF (i.e. large quantities of smaller beads), the small beads support the skeleton exclusively (Fig. 5d,g), and the influence of the large beads on the wave path becomes negligible. Above a critical MF, the addition of more small beads does not significantly alter the wave path and there is no

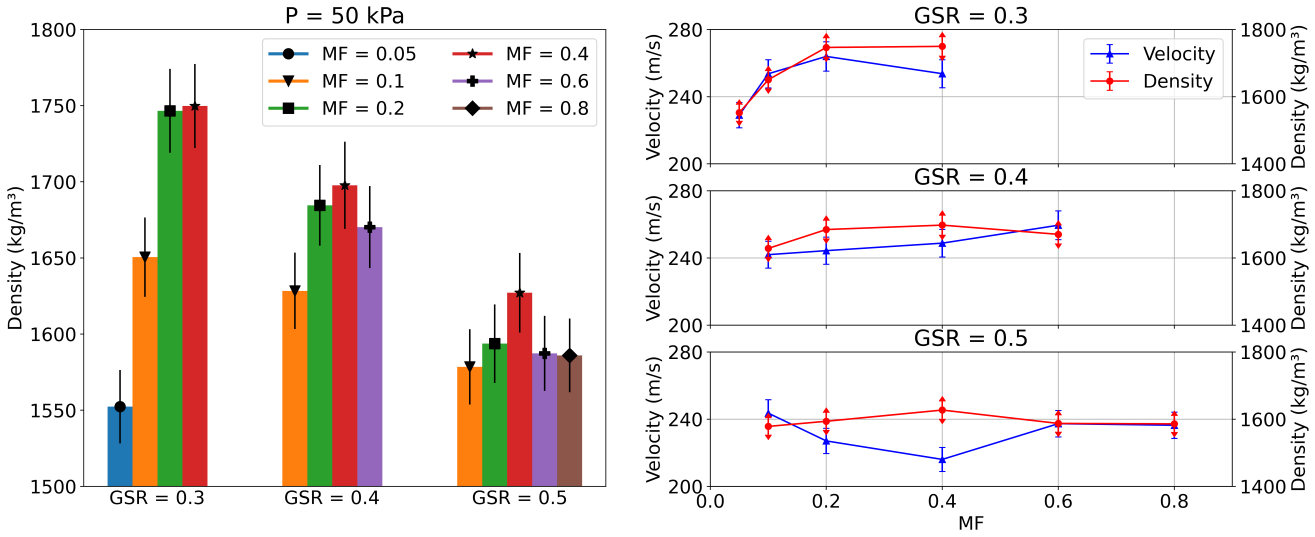


Figure 4: Left: Bulk density with GSR and MF at a 50 kPa confining pressure. Right: Evolution of velocity and density with MF for different GSR at 50 kPa confining pressure.

further impact of increasing MF on the seismic velocity. The critical point at which small beads begin to form the primary component of the skeleton cannot be predicted in advance and is related to the GSR.

At intermediate MF (i.e. similar quantities of large and small beads), the behaviour with increasing MF is highly dependent on the GSR. This is because the capability of the small beads to fill the voids between the large beads is highly dependent on the grain size ratio (GSR), as small beads must be small enough to fill the voids between large beads without significantly altering the skeleton of the large beads. According to a theoretical analysis based on the size of a tetrahedral site in a face-centered cubic packing, Choo et al. (2015) demonstrated that hole filling can occur only if the GSR$\lesssim$0.4 and is not possible otherwise.

**Intermediate MFs at low Grain Size Ratio (GSR$\lesssim$0.4):** As the MF increases, the voids between the large beads are filled by the small beads, thereby shortening the seismic wave path (Fig. 5b). Consequently, both the seismic wave velocity and the bulk density increase. The MF threshold when the hole filling mechanism becomes non negligible for seismic wave path propagation depends on the GSR. If the GSR is very low, many small beads must be added to create adequate bridges between large beads for the wave to propagate (Fig. 5a, where only a few beads cannot generate a link between large beads). Thus, at low GSR, the MF threshold for the appearance of hole filling is significantly high. Conversely, when the GSR approaches 0.4, a few beads suffice to create a shorter route for wave propagation, lowering the MF threshold for hole filling appearance.

With an increasing MF, small beads saturate the gaps, leading to contact rupture between large beads i.e., the large beads are pushed apart by the smaller ones (Fig. 5c). This contact rupture mechanism mainly occurs in high density samples (Choo et al. 2021), which is the case in our study. At low GSR, hole filling and contact rupture may occur simultaneously at different locations within the sample. As a result, there can be competition between the two phenomena; hole filling causes an increase in the seismic velocity while contact rupture has the opposite effect. The MFs at which hole filling dominates vs. when there is competition between hole filling and contact rupture vs. when contact rupture dominates are dependent on the grain size ratio.

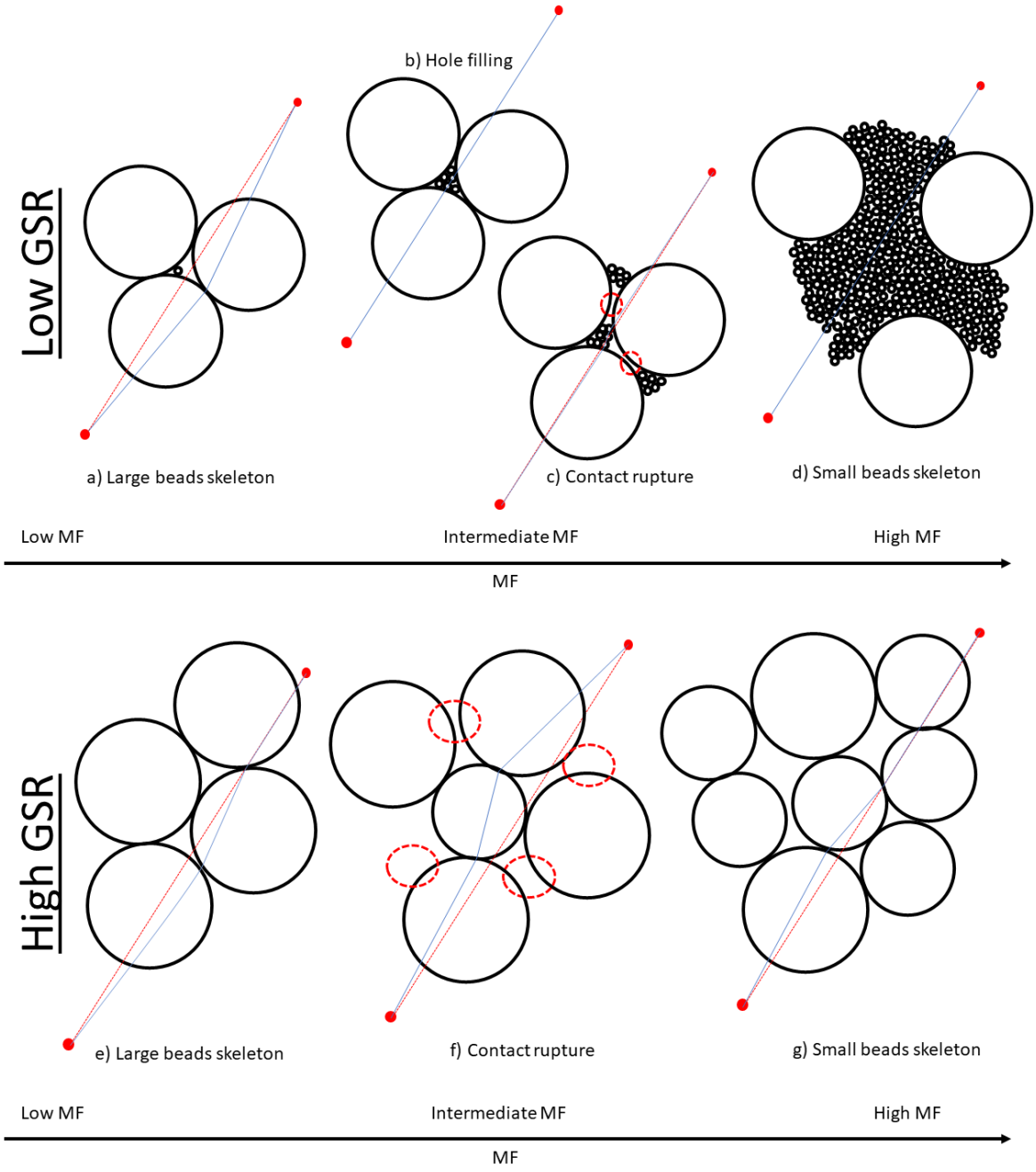


Figure 5: Schematic explaining the influence of the mass fraction (MF) and grain size ratio (GSR) on the seismic velocities. The varying microstructure is shown for low GSR (top) and high GSR (bottom) for MFs increasing from left to right. The seismic wave has to travel from one red point to another. The red line represents the shortest path possible, i.e., a line between the two red points. The blue line represents the shortest path the wave has to go through with the given packing. If there is no red line, then the path taken by the wave is the shortest path.

**Intermediate MFs at high Grain Size Ratio (GSR>0.4):** At high GSR, there is no hole filling because small beads are too large to slip between larger beads. Therefore, only contact rupture occurs as the MF increases and the smaller beads prevent contacts between the larger ones (Fig. 5f). Based on this proposed physical interpretations, Fig. 6 illustrates the evolution of seismic velocity with increasing MF. The mechanisms leading to the velocity trends are also indicated. This is in agreement with observations by Otsubo et al. (2019) and Xie et al. (2023), where large beads skeleton, small bead skeleton and transitional behaviours where dependent on the number of contacts and void ratio variations.

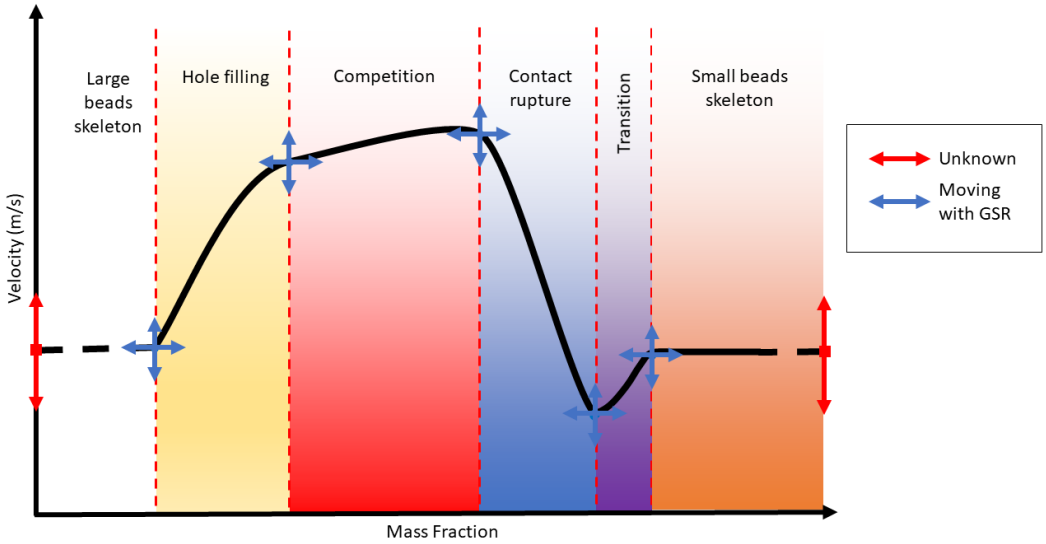


Figure 6: Schematic evolution of the seismic velocity with increasing mass fraction (increasing numbers of smaller beads). The solid black lines are trends supported by the experimental results of this work and explained by the proposed physical interpretations (Fig. 5). The dashed sections of the black line correspond to MFs not tested in this work. The velocity change amplitude and the MF transition between regions varies with GSR. The hole filling mechanism and the competition area only exist for certain GSRs (i.e., theoretically only when GSR$\lesssim$0.4).

## 4.2 Experimental observations

The experimental results are consistent with our hypothetical physical mechanisms influencing the seismic wave velocities. Below we summarize these results.

**Low Grain Size Ratio observations (GSR = 0.3):** At GSR = 0.3, an increase in velocity with MF was observed until MF reached a maximum of 0.2, followed by a decrease thereafter (Fig. 3). We suggest hole filling occurs until MF$\sim$0.2, resulting in both density (Fig. 4) and velocity increases. Then, when MF>0.2, contact rupture starts to dominate, leading to a decrease in velocity whilst density remains constant.

**High Grain Size Ratio observations (GSR = 0.5):** At GSR = 0.5, the velocity decreases with MF until the MF reaches 0.4, but rises again between 0.4 and 0.6, after which it stabilises (Fig. 3). For MF values below 0.4, we suggest that contact rupture dominates as the density experiences a minor increase (Fig. 4) and the velocity undergoes a significant decrease. The velocity increase resulting from the transition between MF = 0.4 and MF = 0.6 suggests that contact rupture stopped and that there are enough small beads to guarantee a faster shear wave propagation. The velocity stability at higher MF values indicates the insensitivity of seismic velocity to MF once the skeleton comprises predominately small beads.

**Intermediate Grain Size Ratio observations (GSR = 0.4):** GSR $\sim$ 0.4 is the threshold for hole filling, and it is, therefore, more difficult to state which mechanism dominates at this GSR. However, the net increase in density between MF = 0.1 and MF = 0.2 when GSR = 0.4 (Fig. 3 and 4) indicates that the hole filling mechanism may be active. We propose that the stability of both velocity and density at higher MFs (Fig. 3) is evidence that there is a competition between hole filling and contact rupture, with each mechanism compensating for the other.

**Velocity variations at constant MF:** The observed change in velocity with GSR, while maintaining a constant MF, is also explicable through microstructural variations. As the GSR increases, the relative size of the small beads increases with respect to the large beads. This favours the contact rupture mechanism resulting in a decrease in velocity with increasing GSR (Fig. 3). Furthermore, we observe that density significantly reduces with GSR whilst maintaining a constant MF (Fig. 4), providing further support for the increasing importance of contact rupture with increasing GSR.

**Sensitivity of velocity to input frequency:** The small increase in velocity with input frequency (Fig. 2) can be interpreted as a stiffening of the medium with increasing frequency (Shapiro et al. 1996). When the frequency is low, the wavelength is greater than the size of the beads, so the waves perceive an averaged medium with no awareness of bead packing. As the frequency increases, the wavelength decreases, and the waves become more sensitive to microstructural variations. Due to this increased sensitivity, the short wavelengths (high frequencies) can then selectively propagate along the shortest chain of beads leading to an increase in the seismic velocity.

# 5 Discussion

The results presented here demonstrate the need to consider multiple influencing factors. Some of the experimental protocol steps could significantly influence the outcome, with the most crucial being the method of sample creation (i.e., filling the membrane). To obtain a homogeneous sample, the ideal approach is to use a zero drop height. A non-zero drop height produces higher density samples in comparison to zero drop height mounted samples (Vaid et al. 1984). Even if our obtained densities are in the range of the first meter of lunar regolith densities, it would have been preferable to obtain bulk densities of 1100 - 1300 kg/m$^3$ to simulate Martian regolith (Grott et al. 2021; Heiken et al. 1991). Furthermore, the sample's homogeneity can be improved. 3D images from our Computed Tomography scans (CT scans) show that the beads are segregated, with smaller beads preferentially located at the bottom of the sample. Nevertheless, our results can still be analysed to determine general trends.

The outcomes of these experiments should be compared with those obtained using monodispersed samples, in order to fully characterize the velocity evolution suggested in Fig. 6 and to determine the behaviour of each bead constituting the binary mix. Additionally, investigating velocity fluctuations that are provoked by modifications in input frequency could be undertaken more exhaustively. For example, the high velocity value at 9 kHz with respect to the one obtained at 6 kHz for GSR = 0.4 and MF = 0.1 (Fig. 2) requires further understanding. Finally, our study was conducted on spherical beads. It would be beneficial to explore the impact of angularity, which is a significant difference between lunar and Martian regolith. Examining sands with varying degrees of angularity could enhance comprehension of the seismic behaviour of planetary regolith (Caicedo et al. 2023). Gravity should also be accounted for in planetary surfaces study.

# 6 Conclusions

Our study was conducted in the GSR range of 0.3 - 0.5. In the future it would be interesting to extend these results to higher and/or lower GSR to confirm the generalization of our findings and proposed physical interpretations. Our findings demonstrate that seismic velocity serves as a marker for microstructural variations in binary mixtures and the associated mechanisms, namely, hole filling and contact rupture. Hole filling involves small beads replacing voids between large beads, resulting in an increased bulk density and a faster transmission of seismic waves. On the other hand, contact rupture occurs when the contacts between large beads are broken due to the presence of small beads, thereby increasing the wave path length and reducing the seismic velocity. The role of contact-breaking on the bulk density is un-

clear.

The study revealed that the outcomes are robust to pressure variations and input frequencies within the ranges tested. It would be worthwhile to confirm whether our findings remain applicable under lower pressure ranges to constrain planetary surfaces with little to no atmospheric pressure. Consequently, seismic velocities measured in-situ on extra-terrestrial bodies will depend on grain size distribution, not just the material density. Therefore, it is crucial to characterise grain size distribution before deducing material macro-parameters from velocity measurement.

# References


Banerdt, W. Bruce et al. (2020). "Initial results from the InSight mission on Mars". In: *Nature Geoscience* 13.3.

Bay, J. A. et al. (1992). "Field and laboratory determination of elastic properties of portland cement concrete using seismic techniques". In: *Transportation Research Record* 1355.

Bernauer, Felix et al. (2020). "Exploring planets and asteroids with 6DoF sensors: Utopia and realism". In: *Earth, Planets and Space* 72.

Blewett, J et al. (2000). "Phase and amplitude responses associated with the measurement of shear-wave velocity in sand by bender elements". In: *Canadian Geotechnical Journal* 37.6.

Brinkman, Nienke et al. (2022). "In Situ Regolith Seismic Velocity Measurement at the InSight Landing Site on Mars". In: *Journal of Geophysical Research: Planets* 127.10.

Brune, James et al. (1963). "Seismic waves and earth structure in the Canadian shield". In: *Bulletin of the Seismological Society of America* 53.1.

Caicedo, B. et al. (2023). "Wave Velocities and Poisson Ratio in a Loose Sandy Martian Regolith Simulant Under Low Stresses: 2. Theoretical Analysis". In: *Journal of Geophysical Research: Planets* 128.11.

Camacho-Tauta, Javier et al. (2012). "A procedure to calibrate and perform the bender element test". In: *Dyna* 79.176.

Carotenuto, Pasquale et al. (2020). "Repeatability of GMAX Bender Element Measurements on Triaxial and Resonant Column Sand Specimens". In: *4th International Symposium on Frontiers in Offshore Geotechnics. Proceedings. (ISFOG)*. Deep Foundations Institute (DFI).

Carrier, W. David (2003). "Particle Size Distribution of Lunar Soil". In: *Journal of Geotechnical and Geoenvironmental Engineering* 129.10.

Cho, Gye-Chun et al. (2006). "Particle Shape Effects on Packing Density, Stiffness, and Strength: Natural and Crushed Sands". In: *Journal of Geotechnical and Geoenvironmental Engineering* 132.5.

Choo, H. et al. (2015). "Shear wave velocity of granular mixtures of silica particles as a function of finer fraction, size ratios and void ratios". In: *Granular Matter* 17.5.

Choo, Hyunwook et al. (2021). "Inverse effect of packing density on shear wave velocity of binary mixed soils with varying size ratios". In: *Journal of Applied Geophysics* 194.

Christensen, Nikolas I. et al. (1995). "Seismic velocity structure and composition of the continental crust: A global view". In: *Journal of Geophysical Research: Solid Earth* 100.B6.

Delage, Pierre et al. (2017). "An Investigation of the Mechanical Properties of Some Martian Regolith Simulants with Respect to the Surface Properties at the InSight Mission Landing Site". In: *Space Science Reviews* 211.1.

Dutta, T. T. et al. (2019). "Stress wave velocity in soils: Apparent grain-size effect and optimum input frequencies". In: *Géotechnique Letters* 9.4.

Dyvik, Rune et al. (1985). "Lab Measurements of $G_{max}$ Using Bender Elements". In: ASCE.

Eberhart-Phillips, D. et al. (1989). "Empirical relationships among seismic velocity, effective pressure, porosity, and clay content in sandstone". In: *GEOPHYSICS* 54.1.

Eggleton, R. A. (2001). *The regolith glossary: surficial geology, soils, and landscapes*. Floreat Park, W.A: Cooperative Research Centre for Landscape Evolution and Mineral Exploration.

Fayon, Lucile et al. (2018). "A Numerical Model of the SEIS Leveling System Transfer Matrix and Resonances: Application to SEIS Rotational Seismology and Dynamic Ground Interaction". In: *Space*

*Science Reviews* 214.8.
Giardini, D. et al. (2020). "The seismicity of Mars". In: *Nature Geoscience* 13.3.
Goetz, W. et al. (2010). "Microscopy analysis of soils at the Phoenix landing site, Mars: Classification of soil particles and description of their optical and magnetic properties". In: *Journal of Geophysical Research: Planets* 115.E8.
Golombek, M et al. (2020). "The origin of sand and dust on Mars: Evidence from the InSight landing site". In: *51st Annual Lunar and Planetary Science Conference*.
Graff, KF (1975). "Wave motion in elastic solids". In: *Publication of: Oxford University Press*.
Grott, M. et al. (2021). "Thermal Conductivity of the Martian Soil at the InSight Landing Site From HP3 Active Heating Experiments". In: *Journal of Geophysical Research: Planets* 126.7.
Heiken, Grant et al. (1991). *Lunar sourcebook: A user's guide to the Moon*. Cup Archive.
Herkenhoff, Kenneth E et al. (2008). "In-situ observations of the physical properties of the Martian surface". In.
Holbrook, W STEVEN et al. (1992). "The seismic velocity structure of the deep continental crust". In: *Continental lower crust* 23.
Lings, M. L. et al. (2001). "A novel bender/extender element for soil testing". In: *Géotechnique* 51.8.
Lognonné, P. et al. (2019). "SEIS: Insight's Seismic Experiment for Internal Structure of Mars". In: *Space Science Reviews* 215.1.
Mayne, PW (2014). "Interpretation of geotechnical parameters from seismic piezocone tests". In: *Proceedings, 3rd international symposium on cone penetration testing*.
McGlynn, Ian O. et al. (2011). "Origin of basaltic soils at Gusev crater, Mars, by aeolian modification of impact-generated sediment". In: *Journal of Geophysical Research: Planets* 116.E7.
Murdoch, N et al. (2015). "Asteroid Surface Geophysics". In: *Asteroids IV*.
Murdoch, N. et al. (2017). "Probing the internal structure of the asteriod Didymoon with a passive seismic investigation". In: *Planetary and Space Science* 144.
Murdoch, N. et al. (2023). "In-Situ Instrumentation for Asteroid Geophysical Exploration". In: *Asteroids, Comets, Meteors Conference*. Houston: Lunar and Planetary Institute.
Nakamura, Yosio et al. (1982). "Apollo Lunar Seismic Experiment—Final summary". In: *Journal of Geophysical Research: Solid Earth* 87.S01.
Otsubo, Masahide et al. (2019). "Particle-scale insight into transitional behaviour of gap-graded materials – small-strain stiffness and frequency response". In: *E3S Web of Conferences* 92. Ed. by A. Tarantino et al.
Robertson, P. K. et al. (1986). "Seismic Cpt to Measure in Situ Shear Wave Velocity". In: *Journal of Geotechnical Engineering* 112.8.
Shapiro, S. A. et al. (1996). "The effect of random isotropic inhomogeneities on the phase velocity of seismic waves". In: *Geophysical Journal International* 127.3.
Sunday, Cecily et al. (2020). "Validating N-body code CHRONO for granular DEM simulations in reduced-gravity environments". In: *Monthly Notices of the Royal Astronomical Society* 498.1.
Vaid, Yoginder Pal et al. (1984). "Relative density of pluviated sand samples". In: *Soils and Foundations* 24.2.
Verdier, N. et al. (2023). "Using Wind Dispersion Effects During the InSight Tether Burial Activities to Better Constrain the Regolith Grain Size Distribution". In: *Journal of Geophysical Research: Planets* 128.5.
Viggiani, G. et al. (1995). "Stiffness of fine-grained soil at very small strains". In: *Géotechnique* 45.2.
Xie, Yipeng et al. (2023). "A quantitative evaluation method for granular skeleton state of binary soils at arbitrary relative density". In: *Computers and Geotechnics* 153.
Yamashita, Satoshi et al. (2009). "Interpretation of International Parallel Test on the Measurement of Gmax Using Bender Elements". In: *Soils and Foundations* 49.4.
Yang, J et al. (2012). *Shear stiffness of granular material at small strains: does it depend on grain size?*
Zimmer, Michael Andrew (2004). *Seismic velocities in unconsolidated sands: Measurements of pressure, sorting, and compaction effects*. Stanford University.